Journal homepage: http://gwse.iheg.org.cn

Research Article

Climate change trends and adaptation strategies in Southern Regions of Iraq

Laheab A Al-Maliki[1*], Rana Abd Al Hadi Mukheef[2], Khaled El-Tawil[3], Nadhir Al-Ansari[4]

[1] *Department of Hydraulic Structures and Water Resources, Faculty of Engineering, University of Kufa, Najaf, Iraq.*
[2] *Civil Engineering Department, College of Engineering, Al-Qasim Green University, Babylon* 51013, *Iraq.*
[3] *Lebanese University, Faculty of Engineering, Beirut, Lebanon.*
[4] *Department of Civil, Environmental and Natural Resources Engineering, Lulea University of Technology, Lulea, Sweden.*

Abstract: This study investigates the impacts of climate change on temperature and precipitation patterns across four governorates in southern Iraq—Basrah, Thi Qar, Al Muthanna, and Messan—using an integrated modeling framework that combines the Long Ashton Research Station Weather Generator (LARS-WG) with three CMIP5-based Global Climate Models (Hadley Centre Global Environmental Model version 2 - Earth System (HadGEM2-ES)), European Community Earth-System Model (EC-Earth), and Model for Interdisciplinary Research on Climate version 5 (MIROC5). Projections were generated for three future time periods (2021–2040, 2041–2060, and 2061–2080) under two Representative Concentration Pathways (RCP4.5 and RCP8.5). By integrating high-resolution climate simulations with localized drought risk analysis, this study provides a detailed outlook on climate change trends in the region. The novelty of this research lies in its high-resolution, station-level analysis and its integration of localized statistical downscaling techniques to enhance the spatial applicability of coarse GCM outputs. Model calibration and validation were performed using historical climate data (1990–2020), resulting in high accuracy across all stations (R^2 = 0.91–0.99; RMSE = 0.19–2.78), thus reinforcing the robustness of the projections. Results indicate a significant rise in average annual maximum and minimum temperatures, with increases ranging from 0.88°C to 3.68°C by the end of the century, particularly under the RCP8.5 scenario. Precipitation patterns exhibit pronounced interannual variability, with the highest predicted increases reaching up to 19.26 mm per season, depending on the model and location. These shifts suggest heightened vulnerability to drought and water scarcity, particularly in already arid regions such as Muthanna and Thi Qar. The findings underscore the urgent need for adaptive strategies in water resource management and agricultural planning, providing decision-makers with region-specific climate insights critical for sustainable development under changing climate conditions.

Keywords: Climate model projections; Climate vulnerability; Extreme events; Hydrological risk; Statistical downscaling

Received: 21 Nov 2024/ Accepted: 03 Sep 2025/ Published: 10 Oct 2025

Introduction

Global warming is proving to be a major problem, especially for the Middle East and North Africa (MENA) region, including Iraq (Namdar et al. 2021; Adamo et al. 2022; Francis and Fonseca, 2024). Climate change impacts are particularly severe and evident in the arid and semi-arid regions of this area. The effects include rising temperatures, shifts in rainfall patterns, and the spread of pests, causing severe environmental and social impacts (Daoudy et al. 2024). These consequences are especially serious for Southern Iraq, which heavily relies on agricultural activity and water supply; it is therefore predicted to experi-

*Corresponding author: Laheab A Al-Maliki, *E-mail address*: laheab.almaliki@uokufa.edu.iq

DOI: 10.26599/JGSE.2025.9280065

AL-MALIKI Laheab A., Mukheef RAAH, El-Tawil K, et al. 2025. Climate change trends and adaptation strategies in Southern Regions of Iraq. Journal of Groundwater Science and Engineering, 13(4): 449-468.

ence rising temperature, increasing water scarcity, and a decline in crop productivity (Al-Maliki et al. 2022; Jasim et al. 2022; Mohammad et al. 2014). These changes are believed to result from increasing emissions of greenhouse gases, such as carbon dioxide, methane, and nitrous oxide, driven by economic development and population growth (Al-Maliki et al. 2022; Hashim et al. 2020).

The strengths of Global Climate Models (GCMs) have been widely acknowledged as a useful means for assessing impacts of climate change and their comprehensiveness (Yildiz et al. 2024; Smirnov et al. 2023; Attogouion et al. 2020; Jahangir et al. 2022). However, GCMs have limitations, primarily in spatial resolution, which is often insufficient to describe small-scale phenomena (Qiu et al. 2022; Lun et al. 2021; Demory et al. 2020) accurately. However, these limitations can be mitigated by using downscaling techniques that help provide more representative data on local weather conditions (Knutti et al. 2010). Dynamical Downscaling and Statistical Downscaling are commonly used (Wang et al. 2022; Wu et al. 2020; Han et al. 2019; Walton et al. 2020).

Previous studies have also employed downscaling methods to estimate the effects of climate change on water resources in certain areas (Portoghese et al. 2015; Hassan et al. 2023; Mohammed and Hassan, 2022). For instance, studies such as Namdar et al. and Francis and Fonseca (2024) highlight regional warming trends that exceed global averages, with increasing frequencies of heatwaves and declining rainfall intensity. Similarly, research by Hassan et al. (2023) and Khalaf et al. (2022) has utilized various climate models and downscaling techniques to simulate future climate scenarios in central and northern Iraq, suggesting significant hydrological impacts and increased drought risk.

Despite this progress, critical research gaps remain, especially in southern Iraq, where few studies have integrated high-resolution climate projections with localized drought risk analysis. Most previous works either lacked adequate spatial resolution or did not comprehensively validate downscaled projections at the station level. Furthermore, few studies have directly linked projected climate trends with practical adaptation strategies for highly vulnerable governorates such as Basrah, Thi Qar, Al Muthanna, and Messan—regions that are agriculturally significant yet increasingly threatened by climate-induced water scarcity.

This research aims to address this knowledge deficiency by providing a detailed prognosis on the climate change trends in the region. It is distinctive in its localized focus on the southern governorates of Iraq, combining high-resolution climate simulations using the LARS-WG weather generator with three global climate models and two emissions scenarios. The work provides a more detailed and validated understanding of projected temperature and precipitation trends than previously available for this region. While the primary focus of this study is to establish localized future climate trends, it also aims to provide a solid basis for future impact-based research in the water and agricultural sectors. The results of this research will expand knowledge about the general effects of climate change, fill a gap in understanding the possible effects in this area, and provide useful information for implementing effective measures to adapt to climate change.

1 Methodology

1.1 Study area

This study focuses on four governorates in southern Iraq: Basrah, Thi Qar, Al Muthanna, and Messan. These regions were selected due to their geological significance and sensitivity to the effects of climate change. Basrah, situated near the Arabian Gulf, is a prominent economic and cultural center, characterized by extensive oil fields and copious farmlands. Thi Qar, located in the southern part of Iraq, has an arid, desert-like terrain, and houses the city of Ur. Al Muthanna lies in the central part of Iraq, primarily consisting of desert landscapes with large dunes and sparse vegetation. Lastly, Maysan, which shares a border with Thi Qar and Iran, is a historically and culturally rich city known for its hot and dry climate. It is a hub for agriculture and the oil sector.

These regions encompass diverse geographical features, including coastal areas, deserts, and riverine zones, each with varying degrees of exposure and vulnerability to climate change impacts, including rising temperatures, shifting precipitation patterns, and increasing water deficiency. Studying these areas together provides valuable insights into the climate change trends and supports the development of targeted adaptation policies in Iraq. Fig. 1 and Table 1 illustrate the locations and coordinates of the study area.

1.1.1 Geological and Hydrogeological Setting

Southern Iraq (Basrah, Thi Qar, Al Muthanna, Maysan) is characterized by predominantly alluvial geology, with Quaternary sand, silt, and clay

Fig. 1 The study area, location map and the selected stations

Table 1 The selected stations

Station	Longitude	Latitude	Elevation
Basra	47.78	30.52	2.0
Thi Qar	46.23	31.02	5.0
Muthanah	45.27	31.27	11.0
Messan	47.17	31.83	9.0

deposits forming horizontally layered aquifers (Namdar et al. 2021). Holocene alluvium dominates near the marshlands, while older Pleistocene and Miocene deposits are found further inland (Al-Ansari et al. 2021). Porosity ranges from moderate to high (25%–35%), but permeability varies significantly across the region (Francis and Fonseca, 2024). Two major aquifer systems exist: Shallow unconfined aquifers at depths of 5–30 m, which are primarily recharged by irrigation and surface water (Al-Ansari et al. 2021), and deeper confined aquifers, located within Miocene-Pliocene formations at depths of 100–300 m (Al-Bahrani et al. 2022). Hydraulic conductivity ranges from 1–10 m/day in sandy areas to <0.1 m/day in clay-rich zones. Specific yields in unconfined zones range from 5% to 15% (Change IPOC, 2007). Groundwater flow generally trends southeastward toward the Shatt al-Arab and the Gulf, influenced by topography and pumping activities (Al-Bahrani et al. 2022; Agyakwah and Lin, 2021). However, local tectonic features such as faults and folds, particularly in Al Muthanna, also affect flow patterns (Francis and Fonseca, 2024). The Tigris and Euphrates rivers (Francis and Fonseca, 2024), along with the Central and Southern Marshes (Al-Hammar, Hawizeh) (Change IPOC, 2007), comprise the primary surface water network, dynamically interacting with the groundwater system. A dendritic drainage pattern (McSweeney et al. 2015), with high infiltration rates in sandy areas, contributes to local recharge. Geological and main hydrogeological zones are presented in Fig. 2, while the groundwater flow maps are shown in Fig. 3.

1.2 LARS-WG model

The Long Ashton Research Station Weather Generator (LARS-WG) is a commonly used model for modeling future climates based on historical climate data. In this study, LARS-WG was

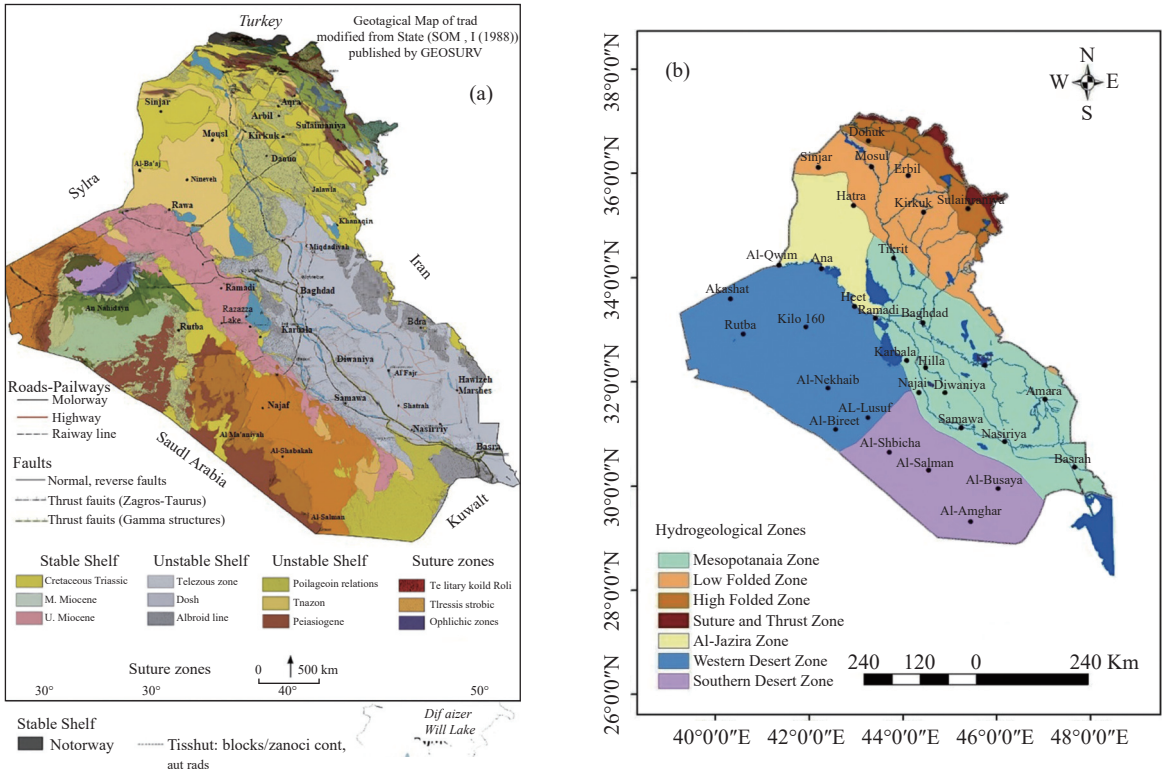

Fig. 2 Geological map of Iraq (Al-Ansari et al. 2021)

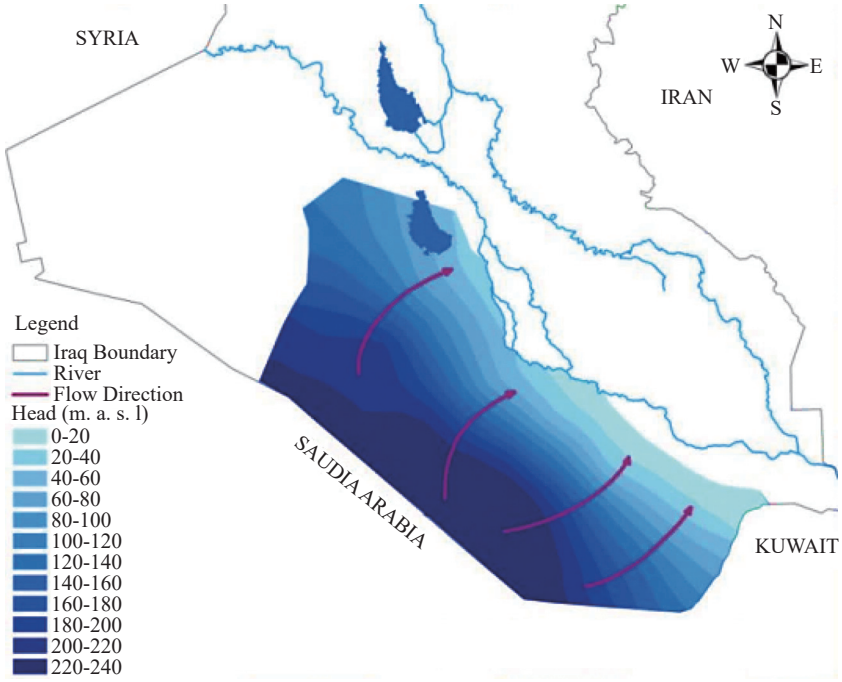

Fig. 3 Groundwater movement in the Southeast part of Iraq (Al-Bahrani et al. 2022)

employed to generate daily time series of temperature and precipitation for the four southern governorates of Iraq: Basrah, Thi Qar, Al Muthanna, and Maysan. This model is particularly suitable for regions with limited or incomplete long-term climate records, as it utilizes a set of statistical parameters derived from observed data to produce synthetic weather sequences (Al-Bahrani et al. 2022).

This study used the LARS-WG to project future climatic conditions in the southern part of Iraq. The parameters, estimated individually for each of the four stations (Basrah, Thi Qar, Al Muthanna, and Messan), include means, standard deviations,

skewness, and lengths of dry and wet spells, as well as transition probabilities between dry and wet days. The choice of these specific parameters reflects their importance for capturing the variability and temporal dependencies within daily weather data, as demonstrated in Hassan et al. (2023). LARS-WG model utilizes a stochastic weather generator to produce daily weather variables, including temperature and rainfall. Another key feature is the utilization of statistical dependencies between observed weather data and the large-scale atmospheric circulation patterns to simulate synthetic weather series for future periods. The model accommodates varying climate conditions by modifying the statistical relationships derived from historical records (Al-Bahrani et al. 2022). Therefore, LARS-WG acts as a vital bridge between large-scale GCM projections and station-level climate impact assessments, highlighting the impracticality of using raw GCM outputs without proper downscaling.

The calibrated LARS-WG was used to develop future climate change projections for the southern region of Iraq using the selected climate change scenarios, based on downscaled global or regional climate models. To evaluate the performance and credibility of the generated climate scenarios, independently observed data were used for validation. An analysis was conducted to determine the level of fit between the model's generated scenarios and the actual climate data, using the coefficient of determination (R^2) and Root Mean Square Error (RMSE) as performance metrics.

The stochastic generation of synthetic weather sequences used a first-order Markov chain model to simulate the occurrence of wet and dry days, while semi-empirical distributions generated precipitation amounts and temperature values. This method effectively preserved the observed variability and inter-variable correlations within the historical data. Bias correction for future climate projections was achieved by applying change factors (delta method) derived from the downscaled outputs of the selected GCMs (detailed below in Table 2). These change factors adjusted the LARS-WG parameters to modify the generated time series for future time horizons. The specific downscaling method employed to obtain the GCM outputs at the required spatial resolution for LARS-WG was a statistical downscaling technique, in which monthly change factors were interpolated to the station level using bilinear interpolation where necessary.

1.3 Global Climate Models (GCMs)

Global Climate Models (GCMs), also known as General Circulation Models, are complex computer-based tools used to simulate and project global climate patterns and changes (Tebaldi and Knutti, 2007). In this study, GCMs were utilized to provide climate projections and insights into future climate scenarios.

1.4 Data input and preprocessing

To apply the LARS-WG model, historical climate data for the study area were collected from meteorological stations and global climate datasets. The data included long-term records of temperature and precipitation. Quality control procedures were conducted to identify and correct any inconsistencies or errors in the data.

1.5 Model evaluation

To assess the performance and reliability of the LARS-WG model, the generated climate scenarios were compared with independent observed data for a validation period. Evaluation metrics, including statistical measures such as Mean Bias Error (MBE) and Root Mean Square Error (RMSE), were calculated to quantify the agreement between the model-generated scenarios and the observed climate data.

The study applied an iterative calibration process to enhance model fidelity. Beyond basic parameter tuning, goodness-of-fit tests (e.g. the Kolmogorov–Smirnov test for rainfall distribution, seasonal assessments for wet and dry periods) were employed to refine the parameter sets. Furthermore, performance was cross-validated using independent datasets, and calibration was repeated if

Table 2 The selected GCMs from the Intergovernmental Panel on Climate Change (IPCC) Models

No.	GCM	Research center	RCP
	MICRO5	Atmosphere and Ocean Research Institute (The University of Tokyo), National Institute for Environmental Studies, and Japan Agency for Marine-Earth Science and Technology, Japan	4.5, 8.5
	HadGEM2-ES	Met Office Hadley Center, United Kingdom	4.5, 8.5
	EC-Earth	European Community Earth-System Model	4.5, 8.5

RMSE exceeded 3 mm for rainfall or 0.3°C for temperature. This rigorous approach ensured that the parameters used were statistically robust and representative of both current and projected climate patterns.

2 Results and discussion

2.1 Calibration and validation of the LARS-WG model

Table 3 presents an assessment of the wet and dry seasons for the four stations: Mesan, Thi-Qar, Basrah, and Muthanah. Each station is evaluated based on the P-value, the Kolmogorov-Smirnov K–S statistic for the wet and dry periods, and the corresponding season (DJF, MAM, JJA, SON).

For Mesan Station, the wet (DJF) and dry (DJF) seasons showed an excellent fit, with P-values of 1.000 and K–S statistics of 0.010 and 0.058, respectively. This pattern continues for the remaining seasons, with strong performance for both wet and dry conditions.

Thi-Qar and Basrah stations exhibited similar results to Mesan, with consistently excellent assessments for wet and dry periods across all seasons.

Muthanah Station also demonstrated a high level of fit, with mostly very good or perfect assessments for wet and dry periods. However, an exception was noted in the dry season (MAM), which had a lower P-value of 0.218 and a higher K–S statistic of 0.297, indicating a relatively weaker match.

These results indicate a high level of consistency between the wet and dry seasons for the four stations. The majority of the assessments are perfect, indicating a strong match between the model outputs and the seasonal wet or dry conditions. However, in some cases, particularly for Muthanah Station during the dry season (MAM), the assessment is relatively weaker, indicating a less consistent relationship between model simulation and the observed wet/dry conditions.

Table 4 presents the results of the K-S (Kolmogorov-Smirnov) test for the daily rainfall distributions at the four stations. For Messan and Thi-Qar Stations, the assessment for January through May were either perfect or very good, with high P-values and low K-S statistics. The assessment for June was rated as good, reflecting a slightly higher K-S statistic, while no precipitation was recorded for July and August. In contrast, September showed a poor fit, with a P-value of 0.000 and a K-S statistic of 1.000. The assessments for October (O), November (N), and December (D) were good to very good.

Table 3 Assessment of wet and dry Seasons for the Four Stations

Season	Wet/dry	N	K–S	*P* value	Assessment
Messan Station					
DJF	Wet	12	0.010	1.000	Perfect
DJF	Dry	12	0.058	1.000	Perfect
MAM	Wet	12	0.050	1.000	Perfect
MAM	Dry	12	0.265	0.341	Poor
JJA	Wet	12	0.000	1.000	Perfect
JJA	Dry	12	0.305	0.193	Poor
SON	Wet	12	0.092	1.000	Perfect
SON	Dry	12	0.083	1.000	Perfect
Thi-Qar Station					
DJF	Wet	12	0.037	1.000	Perfect
DJF	Dry	12	0.055	1.000	Perfect
MAM	Wet	12	0.025	1.000	Perfect
MAM	Dry	12	0.207	0.655	Good
JJA	Wet	12	0.130	0.984	Very good
JJA	Dry	12	0.435	0.017	Poor
SON	Wet	12	0.018	1.000	Perfect
SON	Dry	12	0.098	1.000	Perfect
Basrah Station					
DJF	Wet	12	0.032	1.000	Perfect
DJF	Dry	12	0.065	1.000	Perfect
MAM	Wet	12	0.045	1.000	Perfect
MAM	Dry	12	0.185	0.783	Very good
JJA	Wet	12	0.087	1.000	Perfect
JJA	Dry	12	0.566	0.001	Poor
SON	Wet	12	0.089	1.000	Perfect
SON	Dry	12	0.112	0.997	Very good
Muthanah Station					
DJF	Wet	12	0.062	1.000	Perfect
DJF	Dry	12	0.015	1.000	Perfect
MAM	Wet	12	0.162	0.897	Very good
MAM	Dry	12	0.297	0.218	Poor
JJA	Wet	12	0.174	0.842	Very good
JJA	Dry	12	0.261	0.359	Poor
SON	Wet	12	0.043	1.000	Perfect
SON	Dry	12	0.156	0.920	Very good

Basrah Station received perfect to very good assessments for most months except for June (J) and October (O), which were rated poor, indicating higher K-S statistic. As expected, July (J), August (A), and September (S) recorded no precipitation and November (N) and December (D) again

Table 4 K-S (Kolmogorov-Smirnov) Test for the distributions of daily rainfall for the four studied stations

Season	N	K–S	*P* value	Assessment
Mesan Station				
J	12	0.065	1.000	Perfect
F	12	0.130	0.984	Very good
M	12	0.077	1.000	Perfect
A	12	0.094	1.000	Perfect
M	12	0.223	0.560	Good
J	12	0.652	0.000	Poor
J	12		No precipitation	
A	12		No precipitation	
S	12	1.000	0.000	Poor
O	12	0.219	0.584	Good
N	12	0.130	0.984	Very good
D	12	0.204	0.673	Good
Thi-Qar Station				
J	12	0.142	0.962	Very good
F	12	0.124	0.990	Very good
M	12	0.138	0.971	Very good
A	12	0.135	0.976	Very good
M	12	0.063	1.000	Perfect
J	12	0.348	0.096	Poor
J	12		No precipitation	
A	12		No precipitation	
S	12	0.478	0.006	Poor
O	12	0.146	0.952	Very good
N	12	0.134	0.978	Very good
D	12	0.235	0.492	Good
Basrah Station				
J	12	0.055	1.000	Perfect
F	12	0.085	1.000	Perfect
M	12	0.160	0.905	Very good
A	12	0.043	1.000	Perfect
M	12	0.059	1.000	Perfect
J	12	0.653	0.000	Poor
J	12		No precipitation	
A	12		No precipitation	
S	12		No precipitation	
O	12	0.368	0.067	Poor
N	12	0.147	0.949	Very good
D	12	0.070	1.000	Perfect
Muthanah Station				
J	12	0.156	0.920	Very good
F	12	0.075	1.000	Perfect
M	12	0.104	0.999	Very good
A	12	0.134	0.978	Very good
M	12	0.055	1.000	Perfect
J	12	0.304	0.196	Poor
J	12	No precipitation		
A	12	No precipitation		
S	12	1.000	0.000	Poor
O	12	0.154	0.927	Very good
N	12	0.133	0.979	Very good
D	12	0.056	1.000	Perfect

showed very good fits.

For Muthanah Station, the model achieved very good to perfect assessments for most months, with the exception of June (J) and September (S), which were rated poor due to higher K-S statistics. No precipitation was recorded for July (J) and August (A).

Overall, these results suggest a strong agreement between the simulated and observed daily rainfall distributions at the four stations, with most months showing good to excellent fit. However, in some cases, particularly for Muthanah Station in the dry season (MAM), the fit was poorer, indicating localized discrepancies that may reflect unique climatic variability or data limitations.

To strengthen confidence in LARS-WG's capability to generate future extreme temperature, minimum temperature, and rainfall data, a comparison was made between the statistical outputs obtained from the simulation and those derived from the observed database. Fig. 4 illustrates the graphical comparison of the monthly mean and standard deviation for rainfall, minimum, and maximum temperature generated by LARS-WG and those calculated from historical records in the study area. It is essential to note that previous research has shown that achieving a high degree of agreement between observed and calculated rainfall values is inherently more complex than for temperature, due to intermediate processes such as humidity and cloud formation.

Table 5 and Fig. 5 present the values of the Root Mean Squared Error (RMSE) and Coefficient of Determination (R^2) comparing the observed and simulated data for average monthly temperatures and precipitation at the selected stations. For rainfall, the RMSE values range from 2.0364 to 2.7774, where lower RMSE value indicates a closer match between observed and simulated values. The R^2 values for precipitation range from 0.9188 to 0.9725, representing the proportion of variance in the observed data that is explained by the simulation. Higher R^2 values indicate stronger agreement between the observed and simulated precipitation patterns.

Regarding maximum temperature (T_{max}), the RMSE values are relatively low, ranging from 0.2747 to 0.286138, indicating that the simulated maximum temperature values closely match the observed data. The R^2 values for T_{max} range from 0.9992 to 0.9997, indicating an exceptionally high level of agreement between the observed and simulated temperatures.

Likewise, for minimum temperature (T_{min}), the RMSE values are relatively low, ranging from 0.1904 to 0.2745, indicating a close match between the observed and simulated values. The R^2 values for T_{min} range from 0.9994 to 0.9997, indicating a high level of agreement between the observed and simulated data.

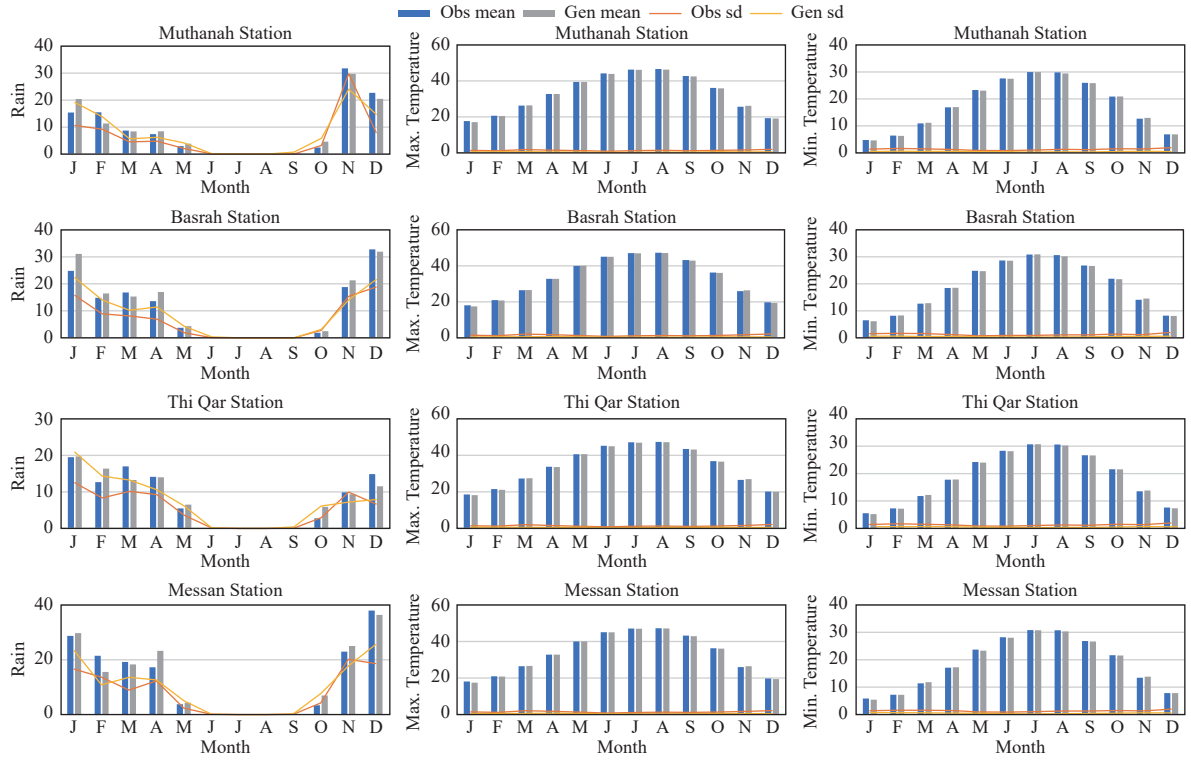

Fig. 4 The monthly mean and standard deviation

Table 5 Statistical analysis of the model calibration and validation over the observation period (1990–2020)

Station	Climate variable	R^2	RMSE
Muthanah	Rainfall	0.9526	2.19823
	T_{max}	0.9994	0.286138
	T_{min}	0.9996	0.1904
Basrah	Rainfall	0.9725	2.3078
	T_{max}	0.9994	0.2747
	T_{min}	0.9997	0.246813
Thi Qar	Rainfall	0.9188	2.0364
	T_{max}	0.9995	0.2755
	T_{min}	0.9994	0.2243
Messan	Rainfall	0.9537	2.7774
	T_{max}	0.9994	0.2747
	T_{min}	0.9992	0.2745

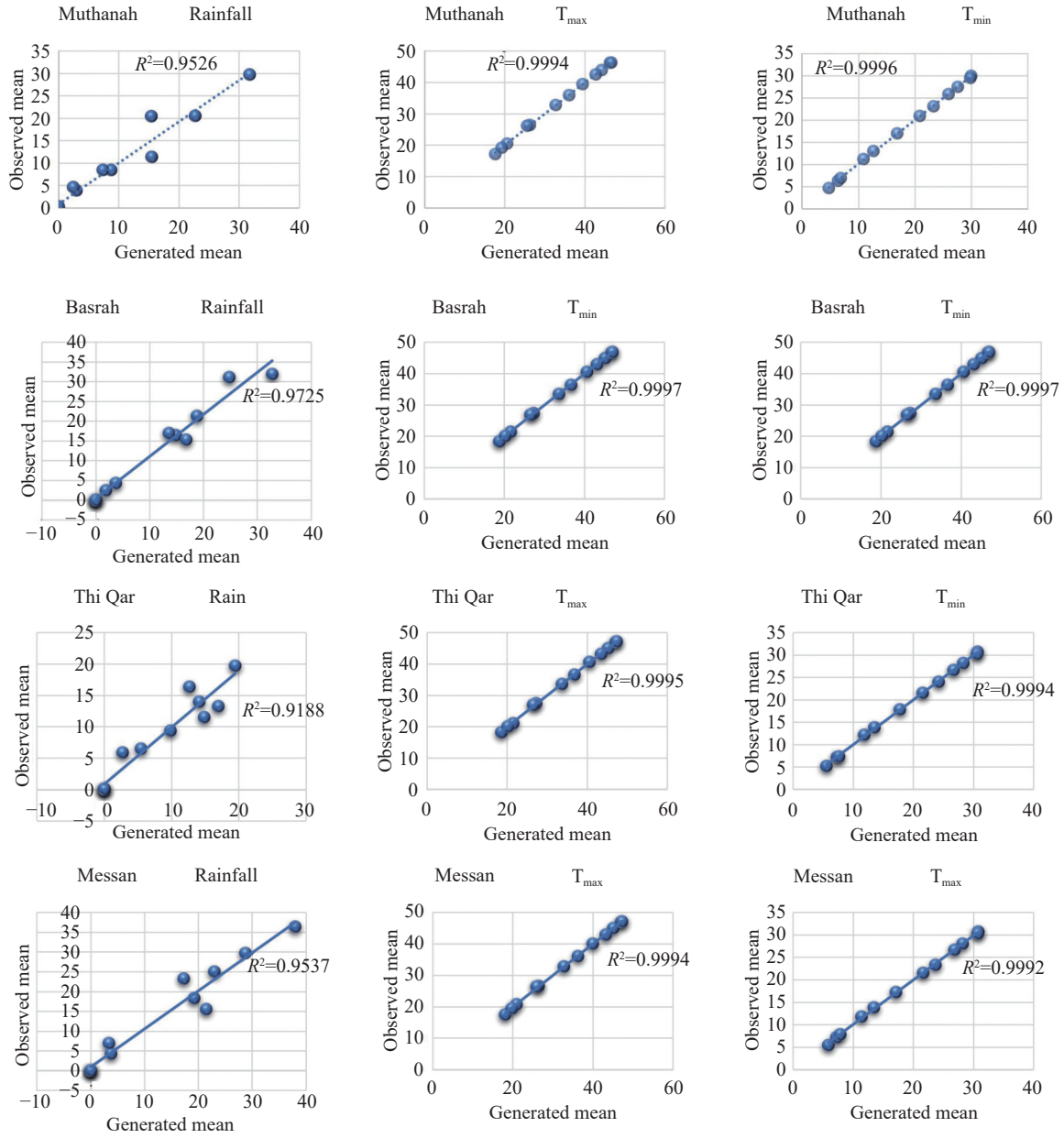

Fig. 5 The coefficient of determination (R^2) between the observed and the simulated data for rainfall, maximum and minimum temperature

Overall, these results confirm that the simulation model performs well in replicating the observed precipitation, maximum temperature, and minimum temperature patterns at the four stations.

While the LARS-WG model demonstrated strong overall performance, a few stations—particularly Muthanna and Basrah—exhibited less satisfactory validation results during specific months (e.g. the MAM and JJA dry seasons). These discrepancies can be attributed to several factors. First, rainfall in these regions is highly sporadic and often concentrated in a few intense events, which introduces challenges in accurately replicating precipitation distribution using stochastic models. Second, the scarcity of summer rainfall, sometimes with months recording no precipitation at all, limits the model's ability to simulate realistic variability, causing high K–S values and low P-values. Third, microclimatic influences, such as local topography and urban heat effects (especially in Basrah), are not fully captured by the statistical parameters of the LARS-WG model. These limitations are common when simulating extremes or low-frequency events in arid and semi-arid climates.

2.2 Future temperature trends

Following the calibrating and validating the LARS-WG model, the weather generator for each selected station (Muthanah, Basrah, Thi Qar, and Messan) was used to predict future daily precipitation, as well as the maximum and minimum temperatures, for the period 2021–2080. This study employed three future time periods: 2021–2040, 2041–2060, and 2061–2080. Projections were based on three GCMs (MICRO5, HadGEM2-ES, and EC-Earth) under the RCP4.5 and RCP8.5 scenarios. Future temperature trends are illustrated in Figs. 6, 7, 8, and 9. Figs. 6 and 7 depict the average monthly maximum and minimum temperatures for the baseline period (1990–2020), as well as the average value of three GCMs expected for each future time period (2021–2040, 2041–2060, and 2061–2080) under RCP4.5 and RCP8.5 scenarios. The results demonstrate a consistent increase in both Tmax and Tmin across all stations and scenarios. The lowest values for Tmax and Tmin were recorded during the baseline period (1990–2020), while the highest values are projected for the 2061–2080 period. January consistently shows the lowest aver-

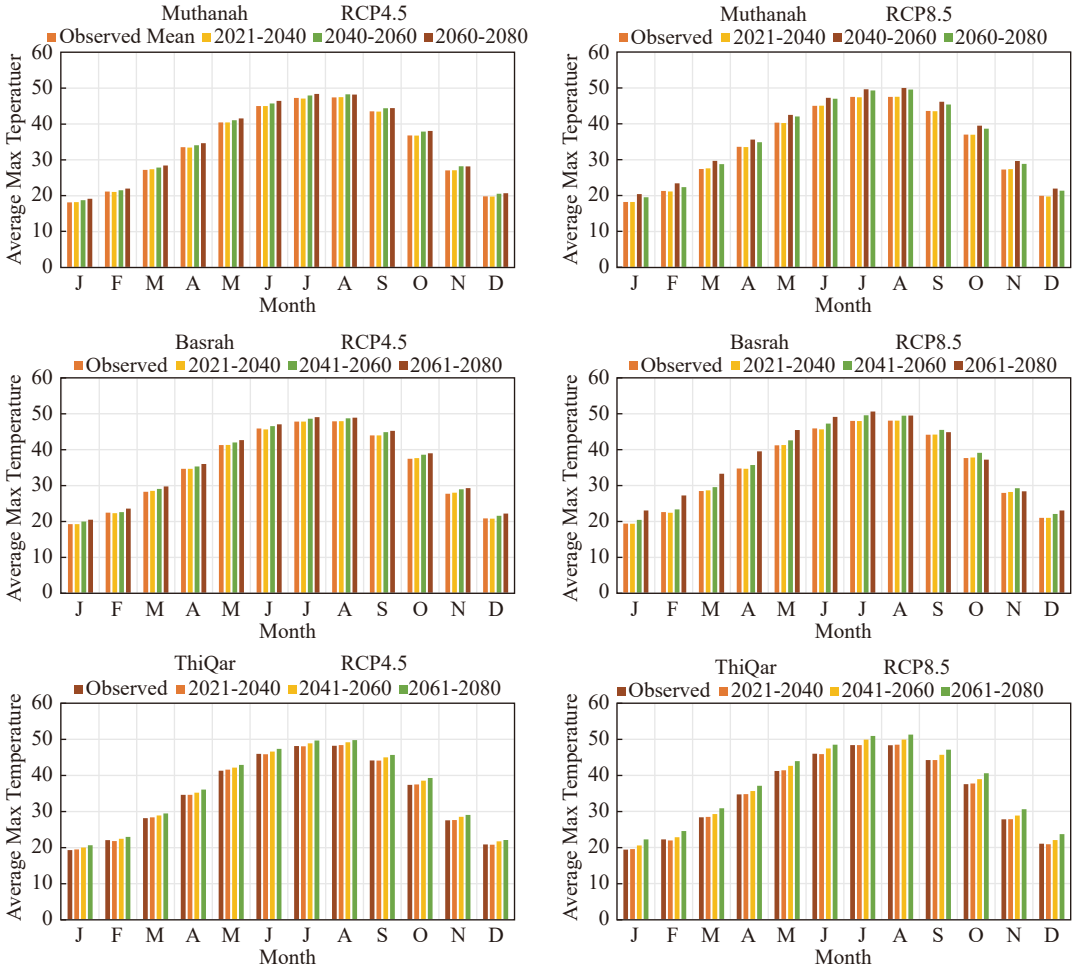

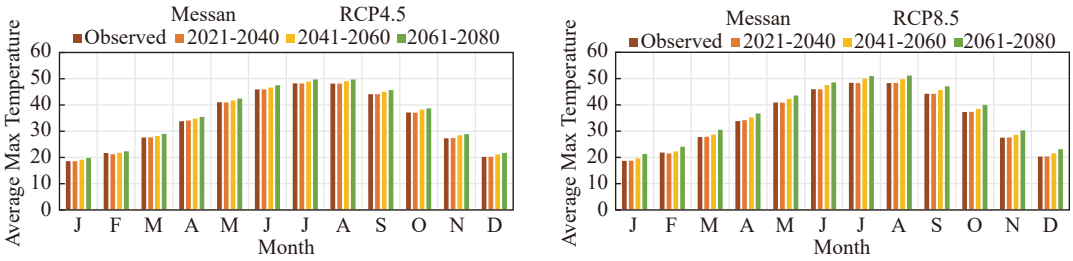

Fig. 6 Average maximum temperatures for observed and simulated data

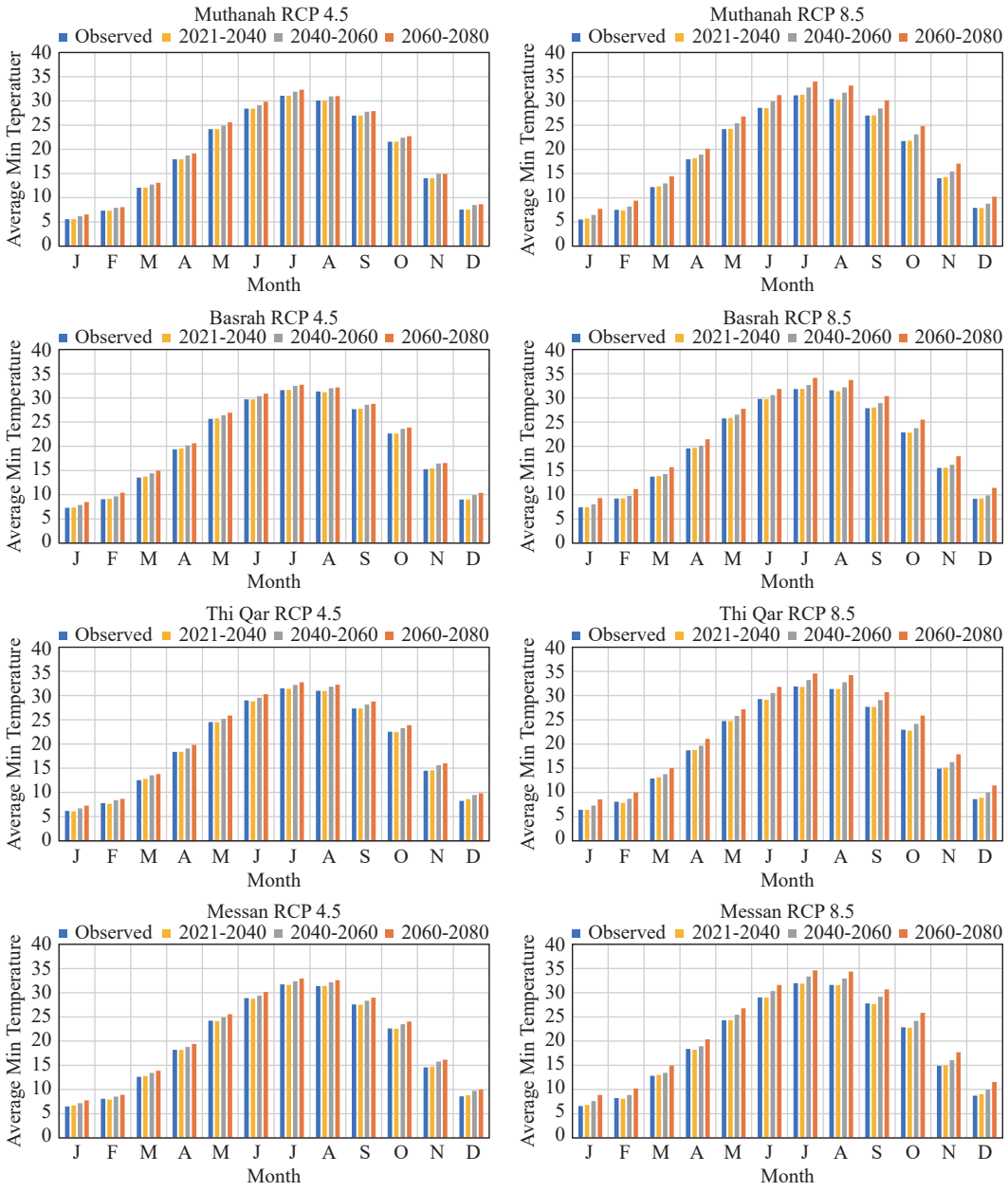

Fig. 7 Average minimum temperatures for observed and simulated data

age temperature, while July and August exhibit the highest temperatures across all four stations. Thi Qar is projected to experience the highest Tmax, with future August temperatures potentially reach 51.28 degrees Celsius by 2061–2080 under RCP 8.5. These findings align with previous studies, such as Mohammed and Hassan (2022).

Figs. 8 and 9 compare the projected minimum and maximum temperatures, respectively. For the three IPCC GCMs under both RCP4.5 and RCP8.5

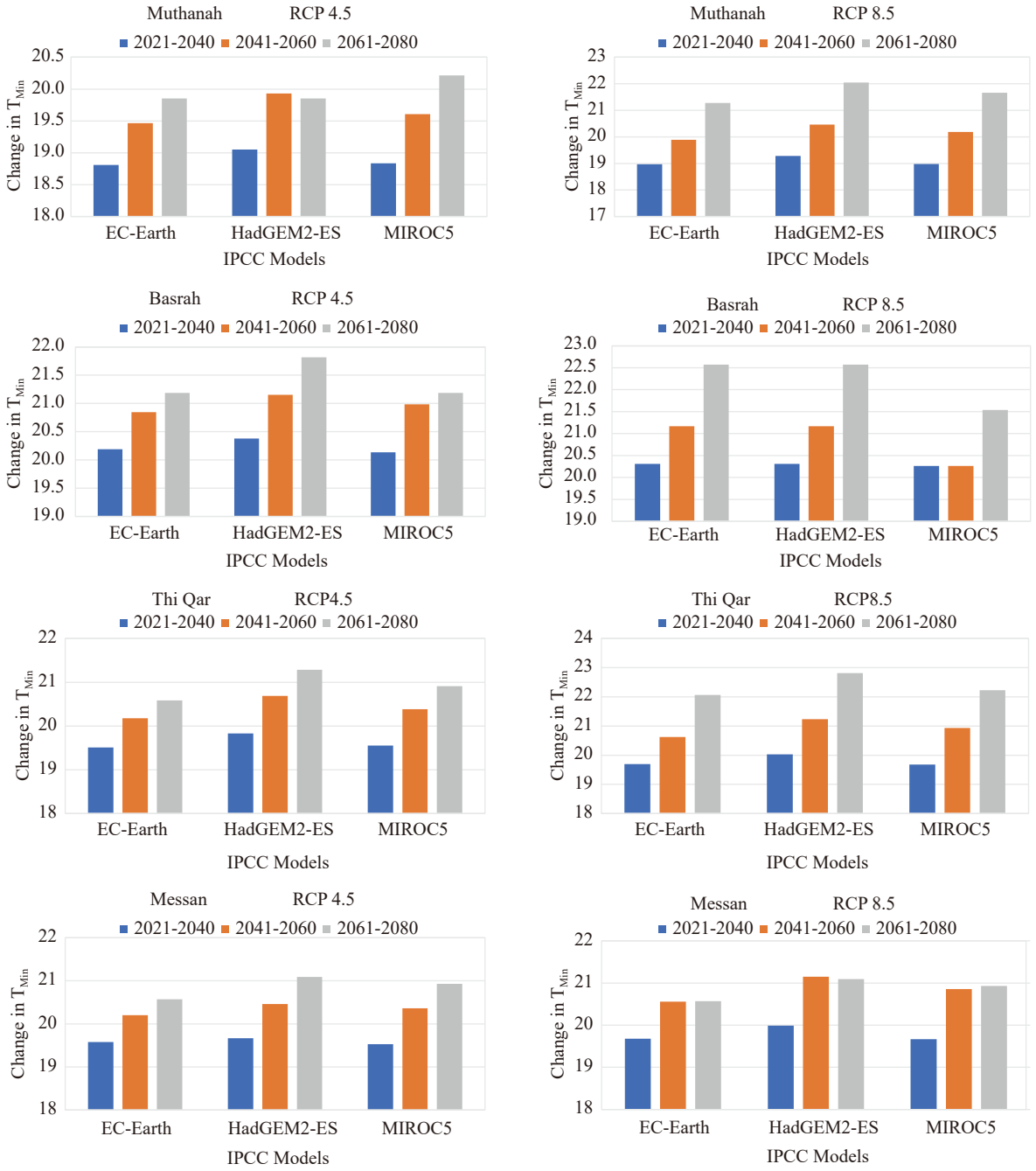

Fig. 8 Comparison of the minimum temperature for the three IPCC models

scenarios. Figs. 10 and 11 further illustrate the differences between the projected minimum and maximum temperatures, respectively, and the reference period for each model and scenario. The highest projected increases in minimum temperature was observed at Basrah for the period

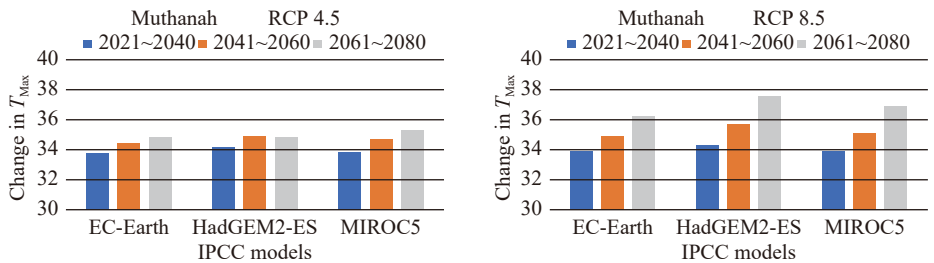

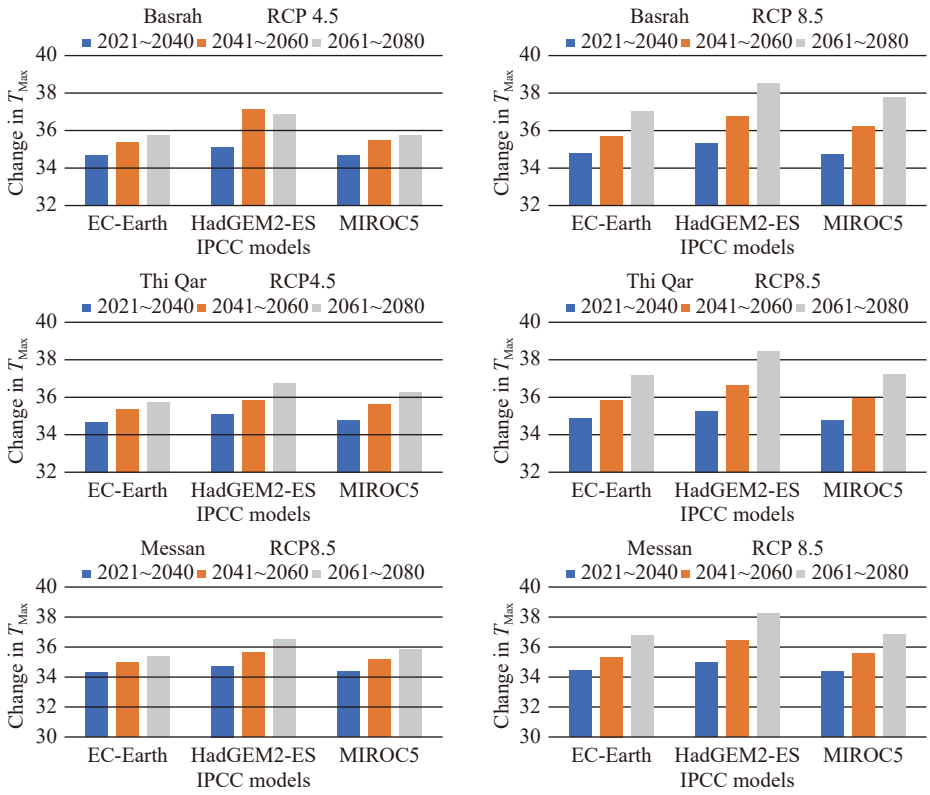

Fig. 9 Comparison of the maximum temperature for the three IPCC models

2061–2080 under RCP 8.5, with an increase of 4.15°C compared to the baseline. Conversely, the smallest increase in minimum temperature was recorded at Thi Qar for the period 2021–2040

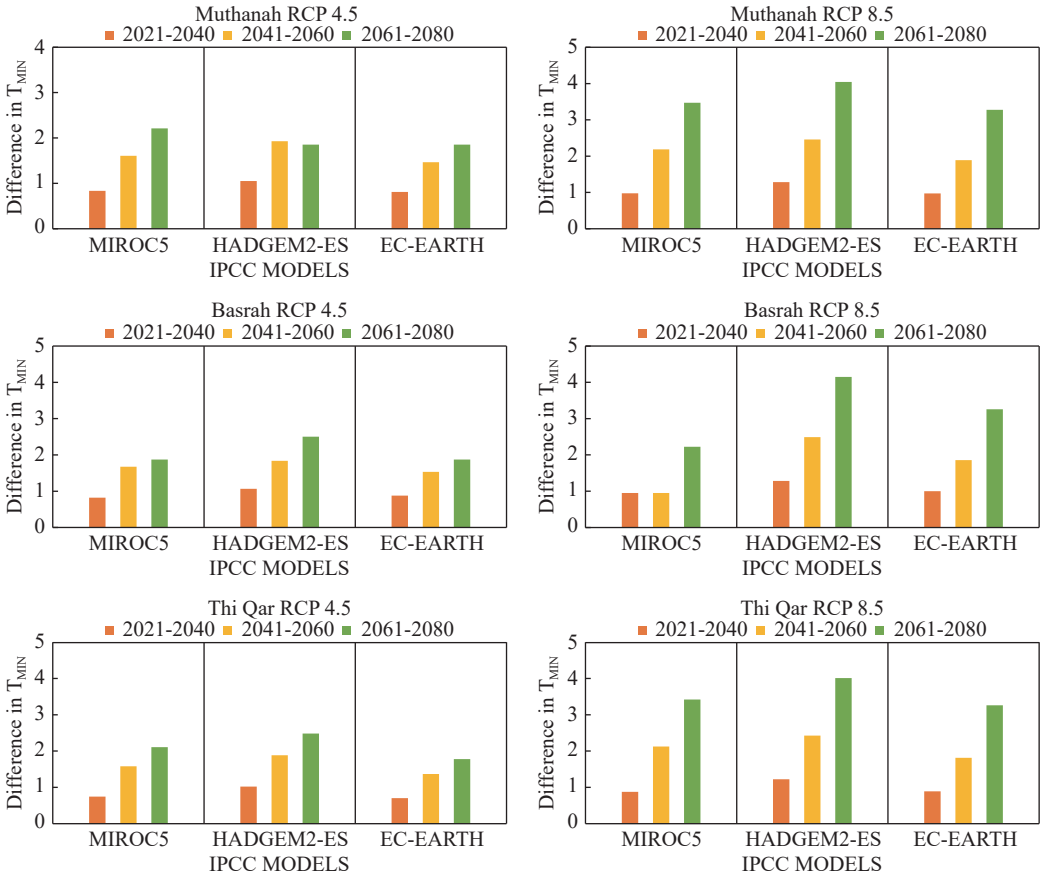

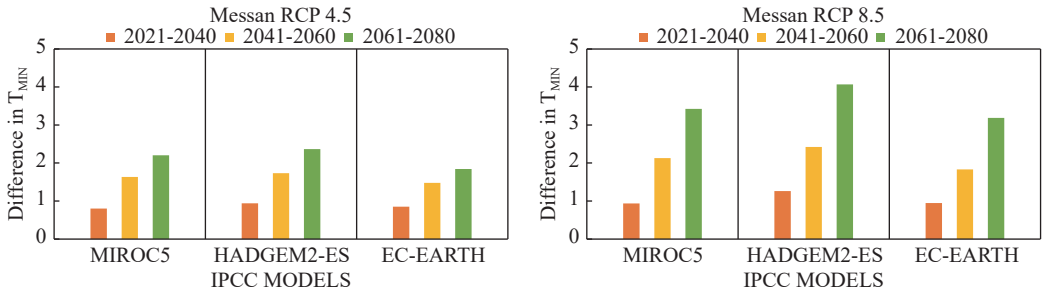

Fig. 10 Annual minimum temperature difference between the simulated values for the three periods and the observed value

under RCP 4.5, with a difference of only 0.7°C. Similarly, for maximum temperature, the largest projected increase was also at Basrah during 2061–2080 under RCP 8.5, reaching a difference of 4.98°C. The smallest increase in maximum temperature was observed at Thi Qar for 2021–

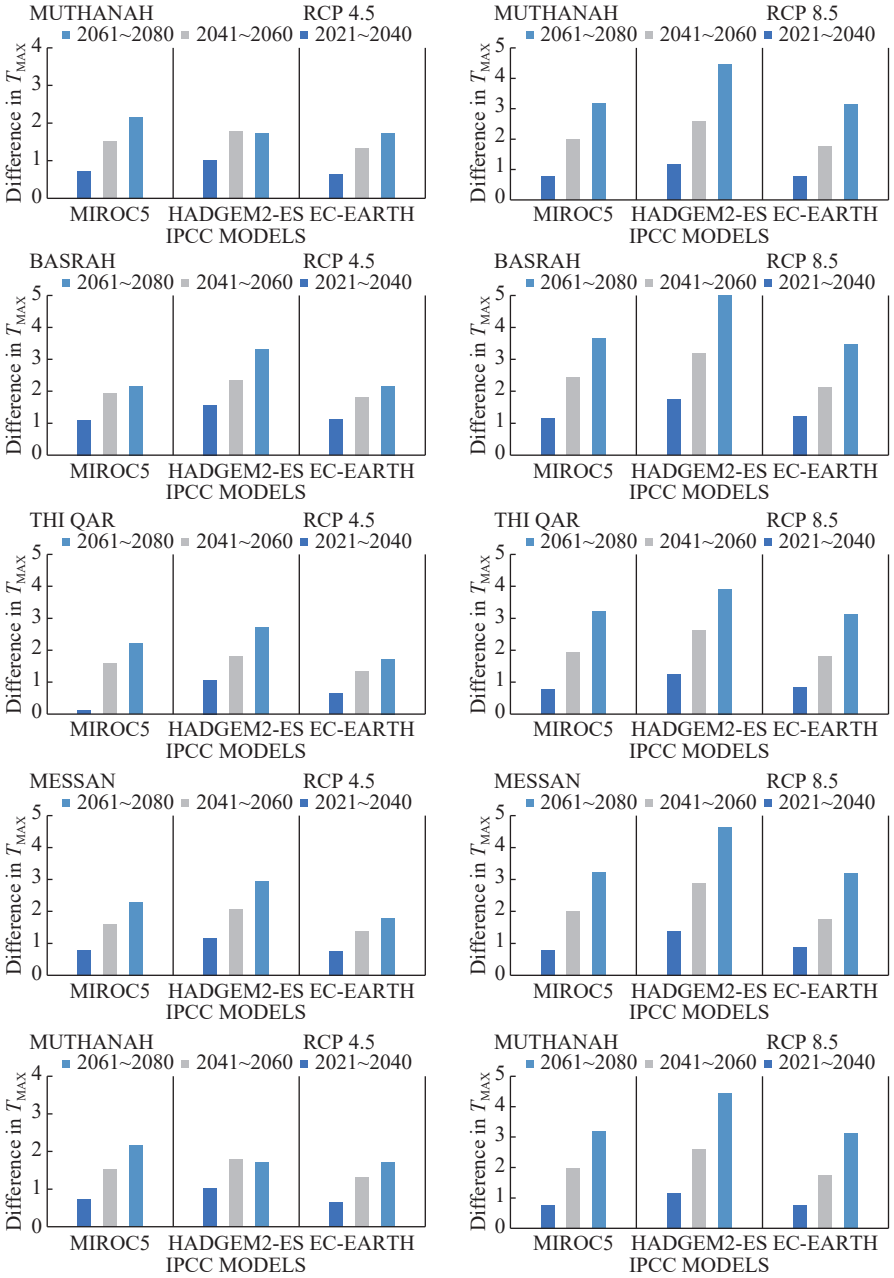

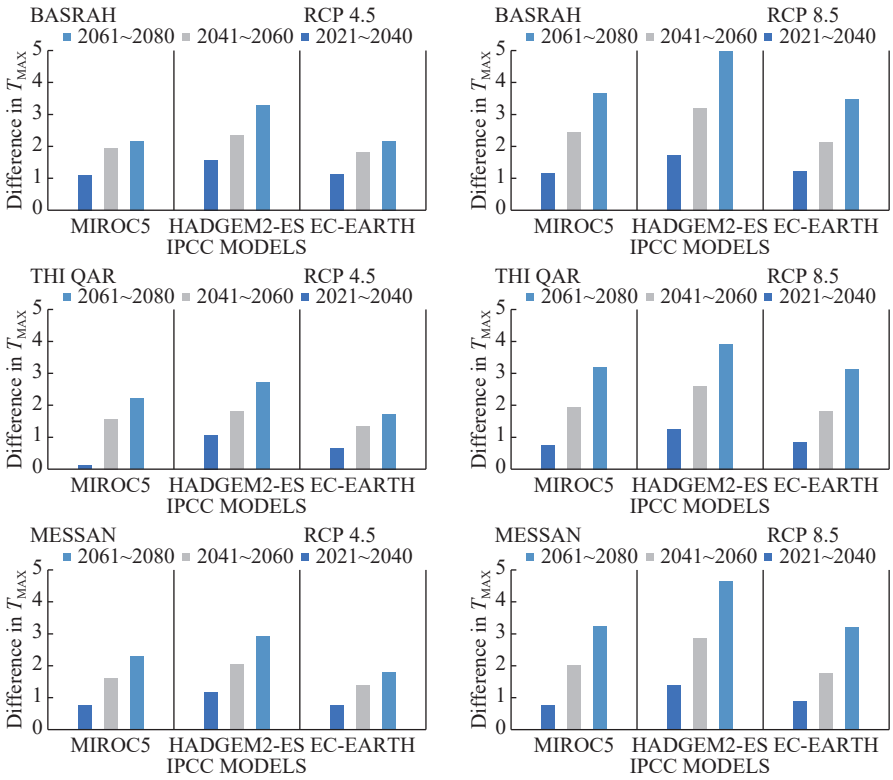

Fig. 11 Annual maximum temperature difference between the simulated values for the three periods and the observed value

2040 under RCP 4.5, with a difference of just 0.11°C.

2.3 Future rainfall trends

Fig. 12 illustrates the observed and predicted average monthly rainfall data for the four selected stations. The results reveal notable temporal and spatial variation in rainfall amounts, distribution, and intensity across the study area. These variations reflect the inherent challenges of capturing consistent precipitation patterns in the region, especially due to minimal or absent rainfall during the summer months. Typically, precipitation shows an increasing trend both annual and monthly during the rainy season (October to May). However, a few months are projected to experience decrease compared to current values in the near future (2021–2040), such as February in Muthanna. Basrah and Thi Qar. For the medium-term period (2041–2060), precipitation generally continues to increase, with exceptions including November in Muthanna and Basrah, October in Thi Qar, and both October and November in Messan.

Fig. 13 illustrates the difference between simulated and observed seasonal rainfall. The results indicated that the highest predicted increase in rainfall was by the HadGEM2-ES model at Basrah under RCP 4.5, with a value of 19.26 mm. The MICRO5 model predicted a maximum increase of 9.25 mm at Messan under RCP 8.5, whereas the EC-Earth model predicted the highest rainfall increase at Muthanah under RCP 8.5, with a value of 11.51 mm. These results align with the those reported by Hassan et al. (2023).

The projected temperature increase for the 21st century across the four selected stations ranges from 0.88°C to 3.68°C (Fig. 14). Fig. 15a and 15b illustrate the spatial distribution of projected temperature changes relative to the historical baseline (1990–2021) and the projected average temperatures under RCP 4.5 and RCP 8.5 scenarios for the period (2021–2080). These findings align with previous research conducted by Hassan et al. (2023).

Although the three GCMs (MIROC5, HadGEM2-ES, and EC-Earth) were all used under the RCP4.5 and RCP8.5 scenarios, their projections exhibit variability in the magnitude and spatial distribution of temperature and precipitation trends across the study area. This inconsistency is expected due to differences in model structure, spatial resolution, and the parameterization of atmospheric and oceanic processes. For instance, MIROC5 tends to simulate relatively wetter conditions in semi-arid regions, while EC-Earth may produce stronger warming signals, particularly during the summer

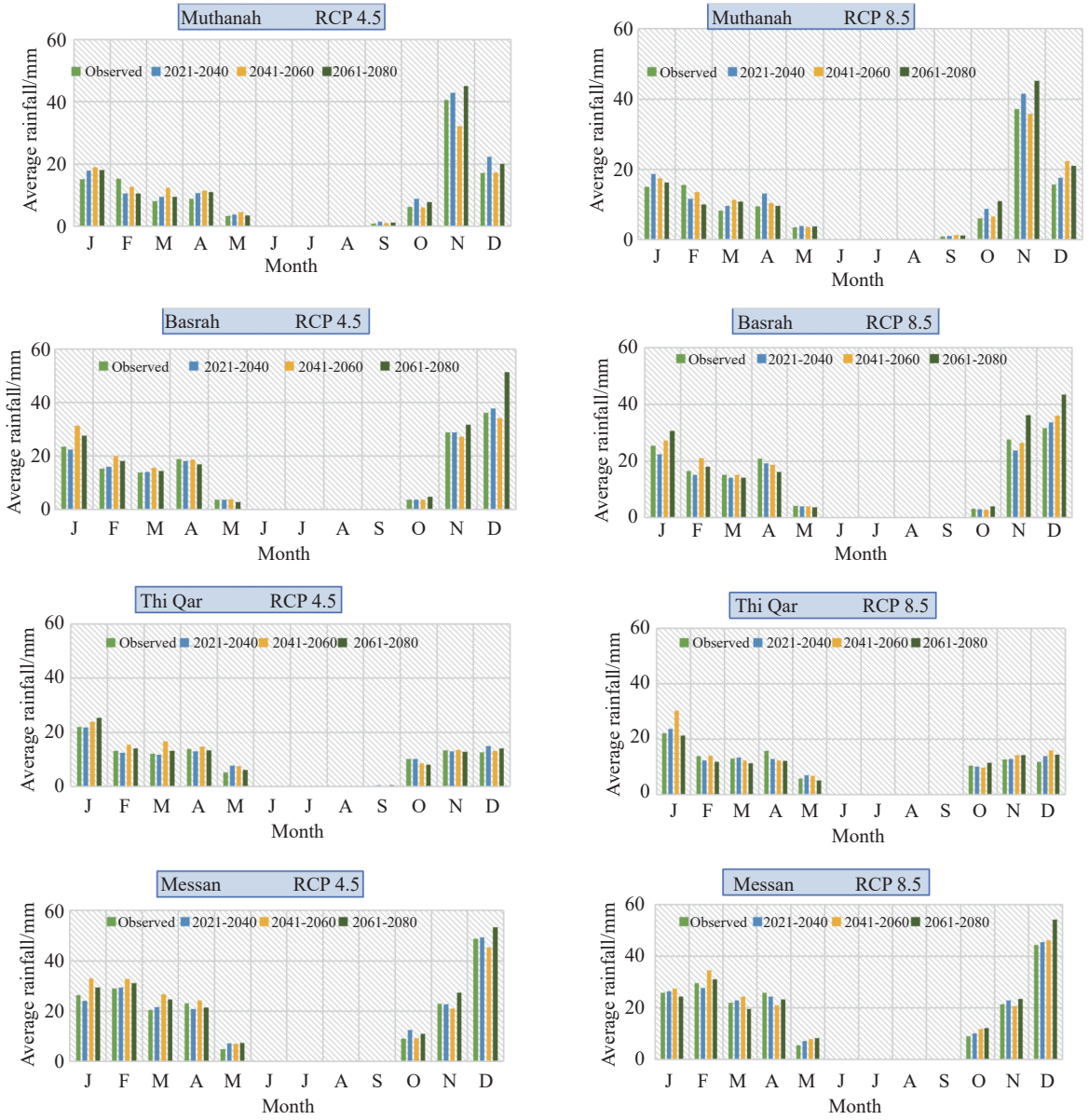

Fig. 12 Average Rainfall for Observed and Simulated Data

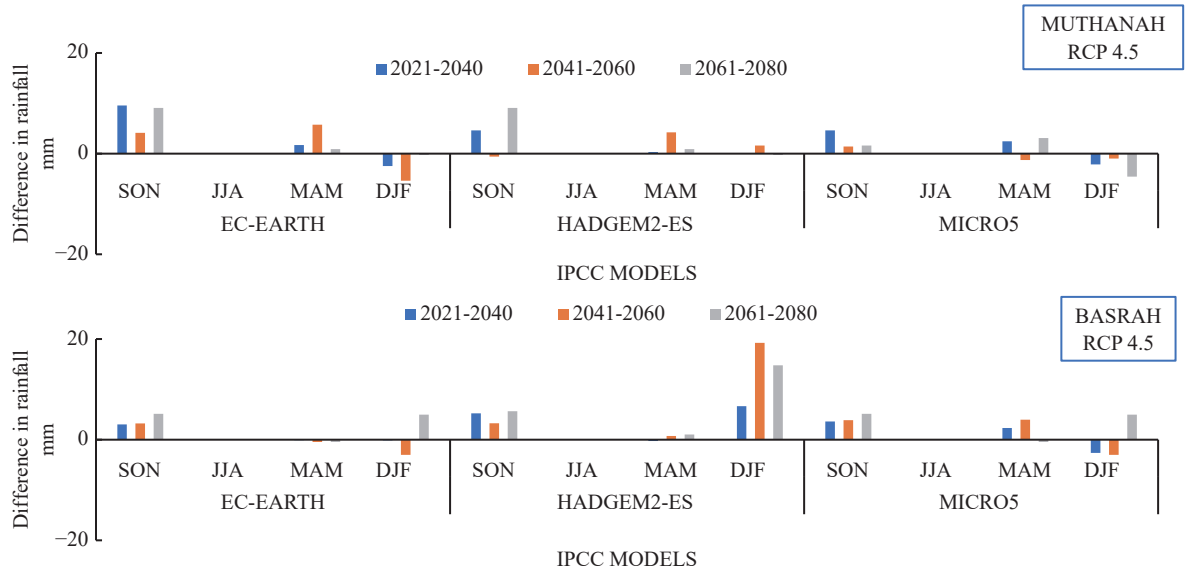

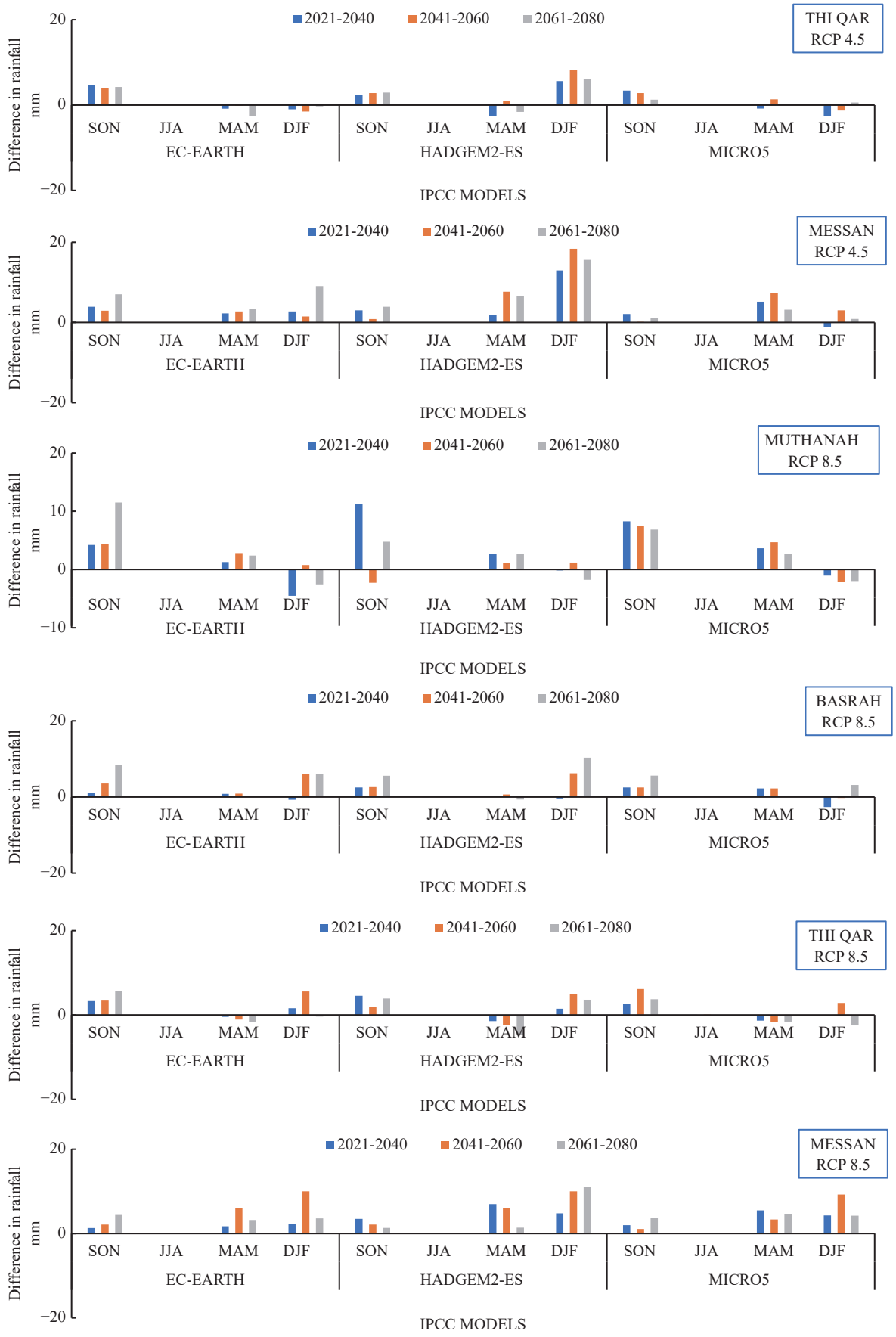

Fig. 13 Difference Between the Simulated and the Observed Seasonal Rainfall

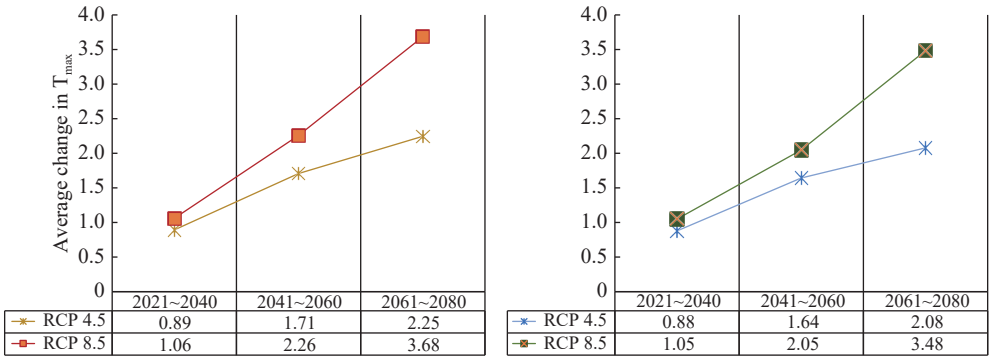

Fig. 14 Alterations in the forecasted annual temperatures in the future of the four stations

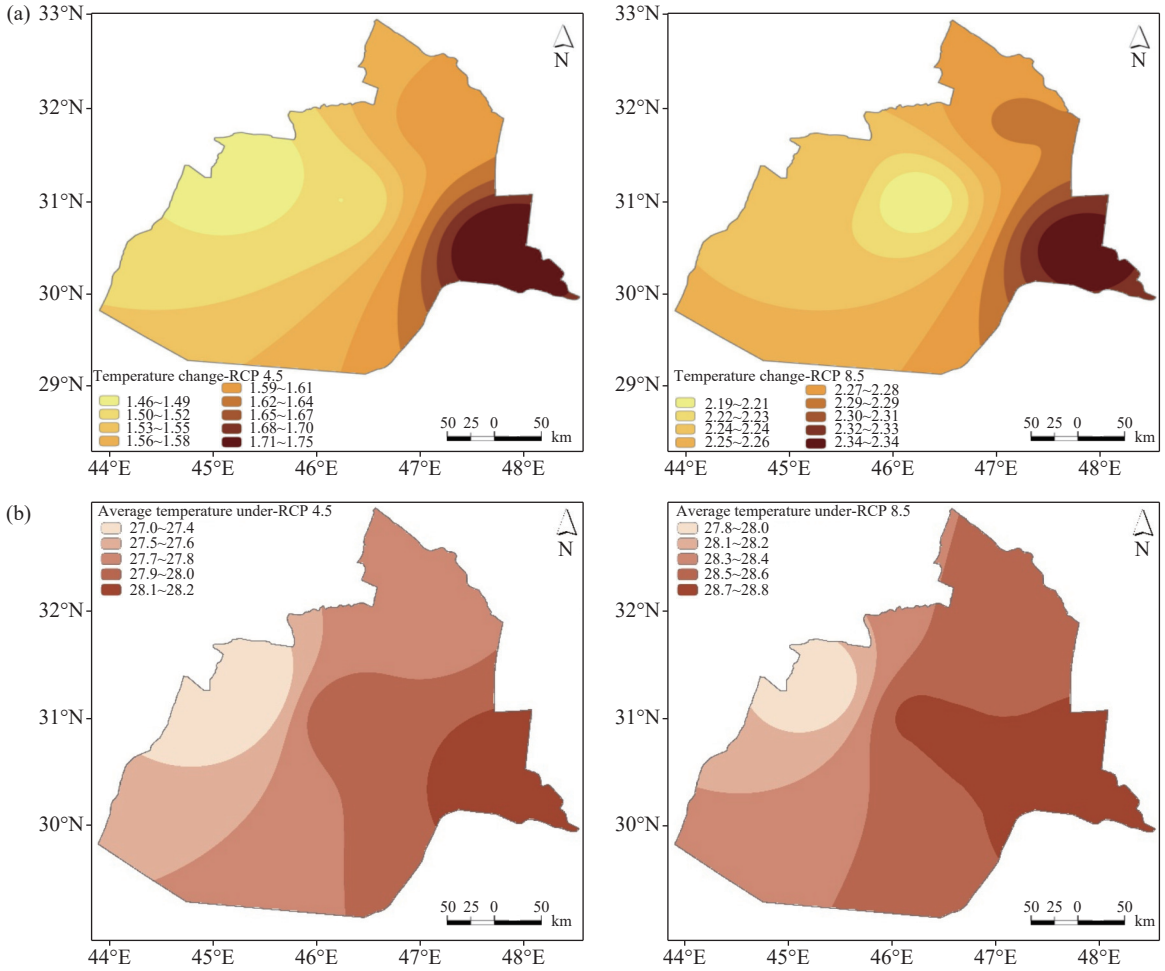

Fig. 15 (a) The spatial distribution of projected temperature changes relative to the historical baseline (1990–2021), and (b) the projected average temperatures under RCP 4.5 and RCP 8.5 scenarios for the future (2021–2080)

months (McSweeney et al. 2015). Rather than relying on a single model, this study adopts a multi-model ensemble approach by analyzing both the average and the range of projections from the three GCMs. This ensemble method enhances the robustness of projections by capturing model uncertainty and providing a more comprehensive picture of future climate conditions (Wilcke and Bärring, 2016; Nolan and Flanagan, 2020). In practice, the ensemble mean represents general trends, while the spread among models highlights potential extremes and informs risk-based adaptation strategies. This approach ensures that planning and policy recommendations are based on a balanced understanding of both best-case and worst-case scenarios.

3 Conclusion and recommendation

3.1 Conclusion

This study examined projected trends in temperature and precipitation across four governorates in southern Iraq—Basrah, Thi Qar, Al Muthanna, and Messan—using the LARS-WG model and three CMIP5-based GCMs under RCP 4.5 and RCP 8.5 scenarios. The results consistently indicate a future increase in both minimum and maximum temperatures, ranging from 0.88°C to 3.68°C by the end of the century. Precipitation patterns exhibit high interannual variability, with some models projecting slight increases during the rainy season, while others suggest continued reduction, especially in already arid regions.

While this study focused on identifying climate trends, it did not explicitly quantify the impacts of these changes on agriculture, water resources, or socio-economic systems. However, the observed warming and fluctuating precipitation patterns imply potential implications for drought risk, crop productivity, and water availability—areas that warrant focused investigation. Future studies should integrate hydrological models, crop models, and socio-economic data to comprehensively assess how these projected climate trends will influence regional water security and agricultural procuctivity.

3.2 Recommendations for future research

Evaluate the hydrological response to changing precipitation and temperature using integrated water balance models.

Investigate the agricultural impacts of projected climate trends by applying crop yield simulation models under different climate scenarios.

Develop localized adaptation strategies informed by both climate projections combined with sector-specific vulnerability assessments.

References

Adamo N, Al-Ansari N, Sissakian V, et al. 2022. Climate change: Droughts and increasing desertification in the Middle East, with special reference to Iraq. Engineering, 14(07): 235−273. DOI：10.4236/eng.2022.147021.

Agyakwah W, Lin YL. 2021. Generation and enhancement mechanisms for extreme orographic rainfall associated with Typhoon Morakot (2009) over the Central Mountain Range of Taiwan. Atmospheric Research, 247: 105160. DOI：10.1016/j.atmosres.2020.105160.

Al-Maliki LA, Al-Mamoori SK, Al-Ansari N, et al. 2022. Climate change impact on water resources of Iraq (a review of literature). IOP Conference Series, Earth and Environmental Science, 1120(1): 012025. DOI：10.1088/1755-1315/1120/1/012025.

Al-Bahrani HS, Al-Rammahi AH, Al-Mamoori SK, et al. 2022. Groundwater detection and classification using remote sensing and GIS in Najaf, Iraq. Groundwater for Sustainable Development, 19: 100838. DOI：10.1016/j.gsd.2022.100838.

Al-Maliki LA, Al-Mamoori SK, Jasim IA, et al. 2022. Perception of climate change effects on water resources: Iraqi undergraduates as a case study. Arabian Journal of Geosciences, 15(6): 503. DOI：10.1007/s12517-022-09695-y.

Al-Ansari N, Saleh S, Abdullah T, et al. 2021. Quality of surface water and groundwater in Iraq. Earth Sciences and Geotechnical Engineering, 11(2): 161−199. DOI：10.47260/jesge/1124.

Attogouinon A, Lawin AE, Deliège JF. 2020. Evaluation of general circulation models over the upper Ouémé River Basin in the Republic of Benin. Hydrology, 7(1): 11. DOI：10.3390/hydrology7010011.

Change IPOC. 2007. Climate change 2007: The physical science basis. Agenda, 6(07): 333.

Daoudy M, Al-Saidi M, Al Manji A, et al. 2024. Troubled waters in conflict and a changing climate: Transboundary Basins across the Middle East and North Africa. Carnegie Endowment for International Peace.

Demory ME, Berthou S, Sørland SL, et al. 2020. Can high-resolution GCMs reach the level of information provided by 12–50 km CORDEX RCMs in terms of daily precipitation distribution? Geoscientific Model Development Discussions, 1-33.

Francis D, Fonseca R. 2024. Recent and projected changes in climate patterns in the Middle East and North Africa (MENA) region. Scientific Reports, 14(1): 10279. DOI：10.1038/s41598-024-60976-w.

Han Z, Shi Y, Wu J, et al. 2019. Combined dynamical and statistical downscaling for high-resolution projections of multiple climate variables in the Beijing–Tianjin–Hebei Region of China. Journal of Applied Meteorology and Climatology, 58(11): 2387-2403.

Hashim BM, Sultan MA, Al Maliki A, et al. 2020. Estimation of greenhouse gases emitted from energy industry (Oil refining and electricity generation) in Iraq using IPCC methodology. Atmosphere, 11(6): 662. DOI：10.3390/atmos11060662.

Hassan WH, Nile BK, Kadhim ZK, et al. 2023. Trends, forecasting and adaptation strategies of climate change in the middle and west regions of Iraq. SN Applied Sciences, 5(12): 312. DOI：10.1007/s42452-023-05544-z.

Jahangir MH, Haghighi P, Danehkar S. 2022. Downscaling climate parameters in Fars province, using models of the fifth report and RCP scenarios. Ecological Informatics, 68: 101558. DOI：10.1016/j.ecoinf.2022.101558.

Jasim IA, Al-Maliki LA, Al-Mamoori SK. 2022. Water corridors management: A case study from Iraq. International Journal of River Basin Management, 1-11. DOI：10.1080/15715124.2022.2079662.

Khalaf RM, Hussein HH, Hassan WH, et al. 2022. Projections of precipitation and temperature in Southern Iraq using a LARS-WG Stochastic weather generator. Physics and Chemistry of the Earth, Parts A/B/C, 128: 103224.

Knutti R, Furrer R, Tebaldi C, et al. 2010. Challenges in combining projections from multiple climate models. Journal of Climate, 23(10): 2739−2758. DOI：10.1175/2009JCLI3361.1.

Lun Y, Liu L, Cheng L, et al. 2021. Assessment of GCMs simulation performance for precipitation and temperature from CMIP5 to CMIP6 over the Tibetan Plateau. International Journal of Climatology, 41(7): 3994−4018. DOI：10.1002/joc.7055.

McSweeney CF, Jones RG, Lee RW. et al. 2015. Selecting CMIP5 GCMs for downscaling over multiple regions. Clim Dyn, 44: 3237–3260. DOI:10.1007/s00382-014-2418-8

Mohammad OI, Laheab A, Al-Maliki. 2014. Evaluation of suitability of drainage water of Al-Hussainia sector (Kut-Iraq) for irrigation. Wasit Journal of Engineering Sciences, 2(1): 30−45. DOI：10.31185/ejuow.Vol2.Iss1.22.

Mohammed ZM, Hassan WH. 2022. Climate change and the projection of future temperature and precipitation in southern Iraq using a LARS-WG model. Modeling Earth Systems and Environment, 8(3): 4205−4218. DOI：10.1007/s40808-022-01358-x.

Namdar R, Karami E, Keshavarz M. 2021. Climate change and vulnerability: The case of MENA countries. ISPRS International Journal of Geo-Information, 10(11): 794. DOI：10.3390/ijgi10110794.

Nolan P, Flanagan J. 2020. High-resolution climate projections for Ireland–a multi-model ensemble approach. Environmental Protection Agency, 978−991. DOI：10.13140/RG.2.2.28360.14084.

Portoghese I, Vurro M, López A. 2015. Assessing the impacts of climate change on water resources: Experiences from the Mediterranean Region.

Qiu Y, Feng J, Yan Z, et al. 2022. High-resolution dynamical downscaling for regional climate projection in Central Asia based on bias-corrected multiple GCMs. Climate Dynamics, 58(3): 777−791.

Smirnov O, Lahav G, Orbell J, et al. 2023. Climate change, drought, and potential environmental migration flows under different policy scenarios. International Migration Review, 57(1): 36−67. DOI：10.1177/01979183221079850.

Tebaldi C, Knutti R. 2007. The use of the multi-model ensemble in probabilistic climate projections. Philosophical Transactions of the Royal Society A: Mathematical, Physical and Engineering Sciences, 365(1857): 2053-2075. DOI：10.1098/rsta.2007.2076.

Walton DB, Berg N, Pierce D, et al. 2020. Understanding differences in California Climate Projections produced by dynamical and statistical downscaling. Journal of Geophysical Research: Atmospheres, 125.

Wang JL, Moore JC, Zhao L, et al. 2022. Regional dynamical and statistical downscaling temperature, humidity and wind speed for the Beijing region under stratospheric aerosol injection geoengineering. Earth System Dynamics, 13(4): 1625-1640.

Wilcke RAI, Bärring L. 2016. Selecting regional climate scenarios for impact modelling studies. Environmental Modelling & Software, 78: 191−201. DOI：10.1016/j.envsoft.2016.01.002.

Wu J, Han Z, Li R, et al. 2020. Changes of extreme climate events and related risk exposures in Huang - Huai - Hai river basin under 1. 5–2°C global warming targets based on high resolution combined dynamical and statistical downscaling dataset. International Journal of Climatology, 41: 1383−1401.

Yildiz S, Islam HMT, Rashid T, et al. 2024. Exploring climate change effects on drought patterns in Bangladesh using Bias-Corrected CMIP6 GCMs. Earth Systems and Environment, 8(1): 21−43. DOI：10.1007/s41748-023-00362-0.